



Structural investigation and giant dielectric response of $\text{CaCu}_3\text{Ti}_4\text{O}_{12}$ ceramic by Nd/Zr co-doping for energy storage applications

Suman Rani¹ · Neetu Ahlawat¹ · Kanta Maan Sangwan¹ · Sunita Rani¹ · R. Punia² · Jaideep Malik³

Received: 4 January 2018 / Accepted: 20 April 2018 / Published online: 26 April 2018
© Springer Science+Business Media, LLC, part of Springer Nature 2018

Abstract

High performance dielectric materials are highly required for practical application for energy storage technologies. In this work, high-k pristine and modified calcium copper titanate having nominal formula $\text{Ca}_{0.95}\text{Nd}_{0.05}\text{Cu}_3\text{Ti}_{4-x}\text{Zr}_x\text{O}_{12}$ ($x = 0.01, 0.03$ & 0.10) were synthesized and characterized for structural and dielectric properties. Single phase formation of the synthesized compositions was confirmed by X-ray diffraction patterns and further analysed using Rietveld refinement technique. Phase purity of the synthesized ceramics was further confirmed by Energy-dispersive X-ray Spectroscopy (EDX) analysis. SEM images demonstrated that grain size of the modified CCTO ceramics was controlled by Zr^{4+} ions due to solute drag effect. Impedance spectroscopy was employed to understand the grain, grain boundaries and electrode contribution to the dielectric response. Nyquist plots were fitted with a 2R-CPE model which confirms the non-ideality of the system. Substitution of specific concentration of Nd and Zr improved the dielectric properties of high dielectric permittivity ($\epsilon' \sim 16,902$) and minimal $\tan\delta$ (≤ 0.10) over a wide frequency range. The giant ϵ' of the investigated system was attributed to internal barrier layer capacitance (IBLC) effect and reduced $\tan\delta$ accredited to enhanced grain boundaries resistance due to substitution of Zr^{4+} ions at Ti^{4+} site.

1 Introduction

In the present age of science, there is increasing attention to miniaturization of electronic devices with efficient performance. For this, continuous interest to develop high performance dielectric materials useful for technological applications. Most of the ferroelectric materials such as barium titanate and lead zirconate titanate exhibits excellent dielectric properties, but change in crystal structure and space group with temperature make them undesirable for many practical applications. Recently, $\text{CaCu}_3\text{Ti}_4\text{O}_{12}$ (CCTO) has been very much famous material due to its high dielectric permittivity ($\epsilon' \sim 10^4$) in single and polycrystalline ceramics, nearly frequency independent up to 1 MHz and without any structural changes in the temperature range 100–400 K [1].

These extraordinary features make CCTO more technical, but one serious drawback is that the loss tangent ($\tan\delta \geq 0.10$) is too high which hinder its many commercial applications. So, investigate to origin of high $\tan\delta$ value and reduce to this value is an urgent issue that should be intensively performed. Generally, solid-state reaction technique is used to synthesize the CCTO from CaCO_3 , CuO , and TiO_2 at high temperatures that accompanys many drawbacks like heterogeneity of precursor materials and long reaction time [2, 3]. Another drawbacks is formation of secondary phases during the synthesis because of limited atomic diffusion through micrometer-sized grains. the presence of secondary phases increase the disorder at the grain boundaries and leads high $\tan\delta$ values [4, 5]. It is well known that the electric properties can be remarkably enhanced when ceramic exhibits homogeneous microstructure. Other effective synthesis methods such as; wet chemistry route, sol–gel, solution combustion synthesis, sonochemical-assisted route, coprecipitation [6–12] and Pechini sol–gel method are available which can improve CCTO characteristics, especially dielectric loss. The another factor that contributing to high $\tan\delta$ in CCTO is the high DC conductivity (σ_{dc}) at lower frequencies which follows the relationship $\tan\delta \approx \sigma_{dc}/\omega\epsilon_0\epsilon'$, where ϵ' is the dielectric permittivity at lower frequencies

✉ Neetu Ahlawat
neetugju@yahoo.co.in

¹ Department of Physics, Guru Jambheshwar University of Science and Technology, Hisar 125001, India

² Department of Physics, Maharshi Dayanand University, Rohtak 1240001, India

³ Department of Chemistry, Indian Institute of Technology, Roorkee 247667, India

[13]. As per IBLC model, the CCTO has electrically heterogeneous microstructure consisting of semiconducting grains isolated by insulating grain boundaries (GBs) and the best approach to minimise the dielectric loss in CCTO is to control the overall insulating properties of the bulk ceramics that might be achieved by increasing GBs layer resistance or via endorsing dense GBs networks [14, 15]. Ion doping in CCTO also found to be effective technique that strongly controls the morphology, particle size, electrical conductivity of grain (conducting/semiconducting nature) and GBs characteristics (thickness, permittivity and resistance) [14, 16]. Each dopant has its own characteristics and affect the microstructure (sintering kinetics and grain growth) as well as modifies the electrical properties of the host system [17]. Therefore, the selection of dopant should be done in such a way that it should tune the grain and GBs characteristics to attain best dielectric results. Rare earth elements (REEs) are lithophile elements that exhibits stable oxidation state (+3) (except for Ce^{+4} and Eu^{2+} in some environments). The stable valence/oxidation state allow for liberal substitution of the REEs into various crystal lattices to alter the existing various properties [18]. To improve the dielectric properties of CCTO, plenty of works have been done on modified CCTO with rare earth ions such as; La^{3+} [19–21], Eu^{3+} [19, 22], Y^{3+} [19, 23], Gd^{3+} [14, 19, 23], Yb^{3+} [24], Sm^{3+} [25] and the dielectric losses were found to be quite low. For example, La^{3+} substitution into CCTO reduced $\tan\delta$ value to be less than 0.03, but simultaneously it worsens other dielectric parameter (large decrease in ϵ' values) also [20]. Recently, Xu et al. reported that co-substitution of rare earth and transition metal (Y + Zr) in CCTO greatly improved the dielectric properties [26]. A very low value of $\tan\delta \sim 0.039$ along with high $\epsilon' \sim 10,196$ was achieved at room temperature at 1 kHz. Nd element exist in Nd^{3+} state and have comparable ionic radii to the Ca^{2+} ions among all the rare earth elements. Wang et al. [27] studied the effects of Nd-substitution on microstructures and dielectric characteristics of CCTO ceramic and observed that both ϵ' and dielectric loss were greatly affected with Nd concentration. Later on, Wang et al. [28] synthesized Nd doped $\text{Ca}_{1-3x/2}\text{Nd}_x\text{Cu}_3\text{Ti}_4\text{O}_{12}$ ceramics and a moderate ϵ' value ($\sim 11,200$) with low $\tan\delta$ (~ 0.12 at 10 kHz) was achieved at room temperature. It is well known that Zr^{4+} cation is more stable than Ti^{4+} cation and substitution of Zr^{4+} at Ti^{4+} ions in perovskite oxide ceramics leads to outstanding dielectric properties for useful applications [29–32]. With this motivation, both Nd^{3+} and Zr^{4+} were simultaneously doped into CCTO matrix and characterised to understand the electrical properties. There are several reports on on separately Nd and Zr doped CCTO ceramics, but, none about the co-substitution of Nd^{3+} and Zr^{4+} ions. Recently, we have studied the composition $\text{Ca}_{0.95}\text{Nd}_{0.05}\text{Cu}_3\text{Ti}_{3.95}\text{Zr}_{0.05}\text{O}_{12}$ co-doped with Nd and Zr and a giant dielectric permittivity ($\epsilon' \sim 19,426$)

with minimal dielectric loss ($\tan\delta \sim 0.067$ at 1 kHz) was achieved [33]. So, the aim of the present work is to explore the concentration of both the ions to get even better dielectric properties. Nd and Zr co-substituted CCTO compositions have been synthesized and effect of concentration of both ions on the microstructure and dielectric properties is investigated in detail.

2 Experimental

Polycrystalline pure and modified CCTO have nominal compositions $\text{Ca}_{0.95}\text{Nd}_{0.05}\text{Cu}_3\text{Ti}_{4-x}\text{Zr}_x\text{O}_{12}$ ($x=0.01, 0.03, \& 0.10$) abbreviated as (CCTO, CCTO1, CCTO2& CCTO3) were synthesized via solid state method. The starting chemicals CaCO_3 (99%), CuO (99%), Nd_2O_3 (99%), TiO_2 (99.9%) and ZrO_2 (99.9%) were taken in stoichiometric ratio, ball milled and then calcined at 1000 °C for 12 h in a conventional furnace. The mixture was dried at hot plate for half an hour. PVA as a binder was added to the mixture to make the pellet of thickness 1–2 mm and diameter ~ 10 mm using uniaxial hydraulic pressing with a pressure of 20 MPa. Sintering was done at 1080 °C for 6 h. X-ray diffraction (XRD) pattern was collected at room temperature using Rigaku Miniflex-II X-Ray Diffractometer with CuK_α ($\lambda = 1.541 \text{ \AA}$) radiation in a wide range of 2θ ($10^\circ < 2\theta < 80^\circ$). Simulations of collected XRD data by the Rietveld profile method using Fullprof software package [34]. Microstructure of fractured surface was observed by scanning electron microscope (Semtrac Mini, Nikkiso, Japan). The elemental composition was confirmed by EDX technique. For electroding, both flat surfaces of the pellets were painted with air-drying conducting silver paste to study the electrical properties. Dielectric measurement was performed using HIOKI 3532-50 LCR HITESTER in the frequency range 100 Hz–5 MHz at room temperature.

3 Result and discussion

3.1 Structural and microstructure analysis

X-ray diffraction patterns along with a magnified view of most intense diffraction peak ($\sim 2\theta = 34^\circ$) for all the modified CCTO compositions are shown in Fig. 1. The well defined diffraction peaks without any secondary phase indicate that substituted dopants occupies their assigned site and did not influenced the crystal symmetry. Further, XRD data were analysed to calculate the lattice parameters for all compositions using Rietveld refinement. CCTO are known to have double perovskite cubic structure described by the space group $\text{Im}\bar{3}$ [1]. The refinement of the collected XRD data was performed using cubic crystal symmetry with space group

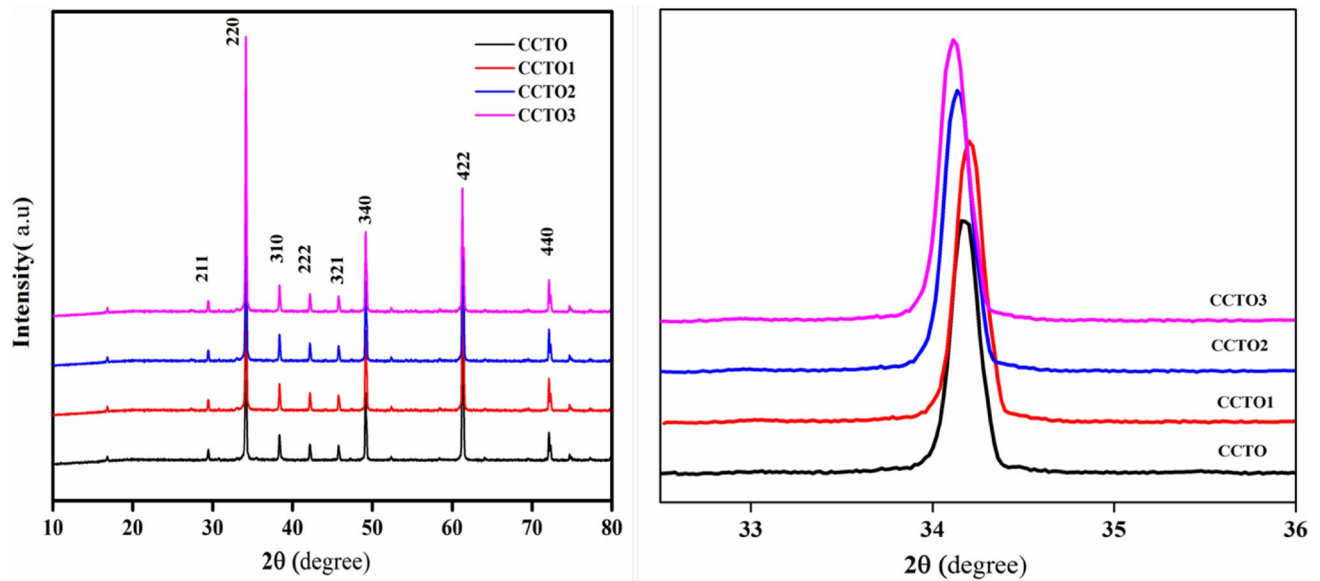


Fig. 1 X-ray diffraction pattern of the pure CCTO and $\text{Ca}_{0.95}\text{Nd}_{0.05}\text{Cu}_3\text{Ti}_{4-x}\text{Zr}_x\text{O}_{12}$ ($x=0.01, 0.03$ & 0.10) ceramics recorded at room temperature alongwith magnified view of peak at around $2\theta \sim 34.19^\circ$

Initially, the zero point shift, unit cell and background and then all input parameters required for the simulation were refined. Pseudo-Voigt function was employed to fit the diffraction peak profile. Rietveld refined X-ray pattern of all prepared compositions are shown in Fig. 2. A low value of goodness of fit (χ^2) factor for all the compositions indicates good fitting between the theoretical and experimental data and refined structural parameters are listed in Table 1. A small decrease in lattice parameters and unit cell volume was observed for CCTO1 ceramic as compared to pure CCTO

might be due to substitution of effective small ionic radii of Nd^{3+} (1.27 \AA) at Ca^{2+} (1.35 \AA) site. For CCTO2 and CCTO3 ceramics the trend is reversed because of the dominance effect of Zr^{4+} ions at Ti^{4+} site. The average crystallite size (D) was estimated by Debye Scherrer formula, for highly intense diffraction peak (at around $\sim 2\theta = 34^\circ$).

$$D = \frac{K\lambda}{\beta \cos \theta} \quad (1)$$

Table 1 Rietveld refined structural parameters and profile R-factors for undoped CCTO and doped namely CCTO1, CCTO2 and CCTO3 ceramics

| Sample | Crystal structure | Cell parameters | Atoms | Position coordinates | | | Profile R-factors |
|--------|-------------------|---|-------|----------------------|--------|------|--|
| | | | | x | y | z | |
| CCTO | Cubic | $a = 7.3897 \text{ \AA}$ $V = 403.548 \text{ \AA}^3$ | Ca | 0 | 0 | 0 | Rp = 3.998 Rwp = 6.204 $\chi^2 = 3.30$ |
| | | | Cu | 0 | 0.50 | 0.50 | |
| | | | Ti | 0.25 | 0.25 | 0.25 | |
| | | | O | 0.1649 | 0.3067 | 0.00 | |
| CCTO1 | Cubic | $a = 7.3890 \text{ \AA}$ $V = 403.419 \text{ \AA}^3$ | Ca/Nd | 0 | 0 | 0 | Rp = 4.07 Rwp = 5.90 $\chi^2 = 3.11$ |
| | | | Cu | 0 | 0.50 | 0.50 | |
| | | | Ti/Zr | 0.25 | 0.25 | 0.25 | |
| | | | O | 0.1744 | 0.3043 | 0.00 | |
| CCTO2 | Cubic | $a = 7.3911 \text{ \AA}$ $V = 403.763 \text{ \AA}^3$ | Ca/Nd | 0 | 0 | 0 | Rp = 5.98 Rwp = 8.80 $\chi^2 = 3.19$ |
| | | | Cu | 0 | 0.50 | 0.50 | |
| | | | Ti/Zr | 0.25 | 0.25 | 0.25 | |
| | | | O | 0.1812 | 0.3298 | 0.00 | |
| CCTO3 | Cubic | $a = 7.3917 \text{ \AA}$ $V = 403.862 \text{ \AA}^3$ | Ca/Nd | 0 | 0 | 0 | Rp = 4.94 Rwp = 5.89 $\chi^2 = 2.96$ |
| | | | Cu | 0 | 0.50 | 0.50 | |
| | | | Ti/Zr | 0.25 | 0.25 | 0.25 | |
| | | | O | 0.1840 | 0.3124 | 0.00 | |

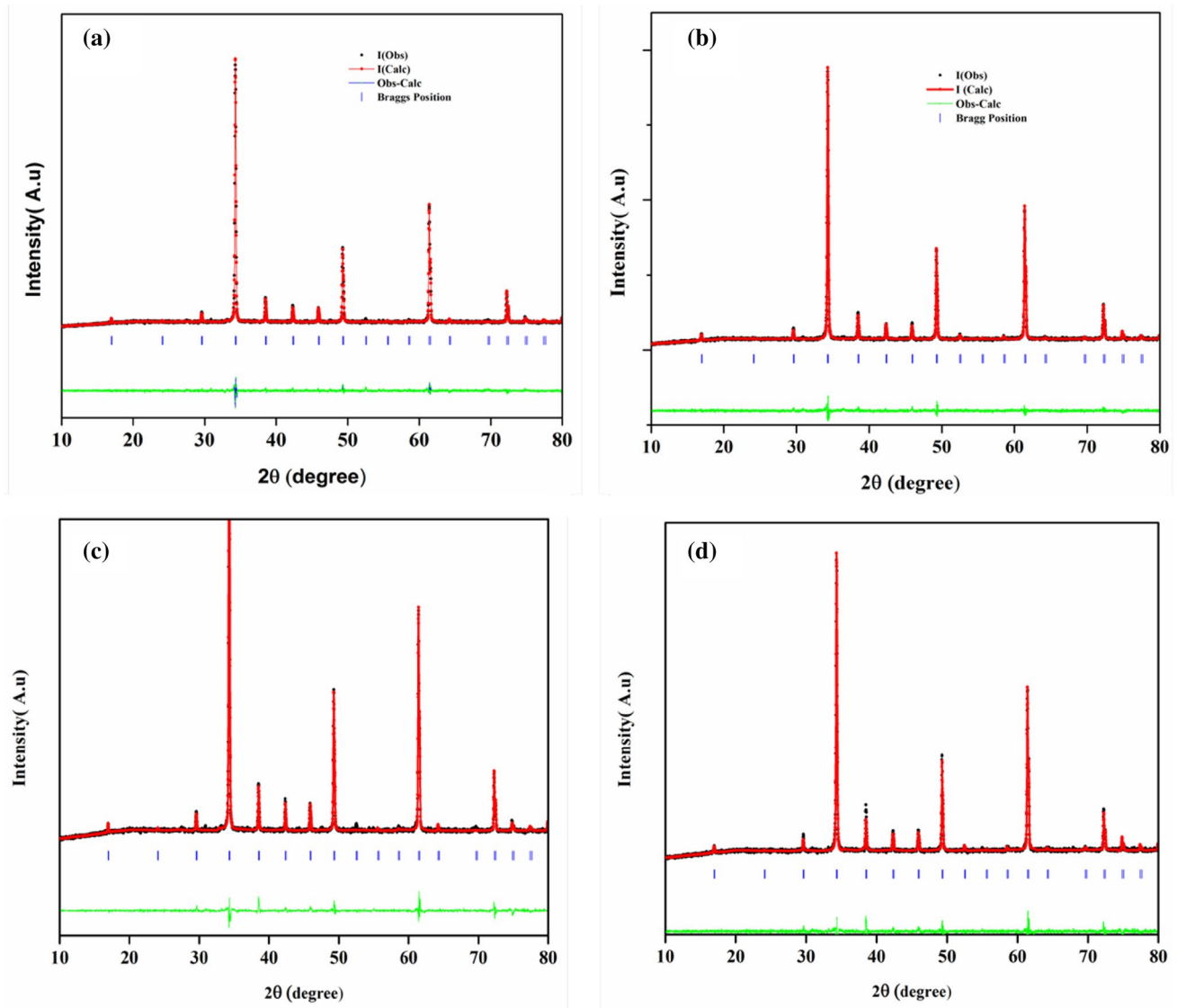


Fig. 2 Rietveld refined patterns of X-ray diffraction data of **a** CCTO, **b** CCTO1, **c** CCTO2 and **d** CCTO3 ceramics

Table 2 Summary of structural data of crystallite size (D), X-ray density (d_x), Experimental bulk density (d_{exp}), porosity (P) and grain size for all the CCTO compositions

| Sample | D (nm) | d_x (g/cm ³) | d_{exp} (g/cm ³) | P (%) | Grain size (μm) |
|--------|--------|----------------------------|--------------------------------|-------|-----------------|
| CCTO | 74 | 5.08 | 4.96 | 3.0 | 7.48 |
| CCTO1 | 75 | 5.11 | 4.90 | 5.0 | 7.43 |
| CCTO2 | 58 | 5.12 | 4.92 | 4.3 | 4.16 |
| CCTO3 | 59 | 5.19 | 5.02 | 3.2 | 2.84 |

where, $K \sim 0.9$ (constant), θ is the Bragg's angle and β is Full Width Half Maxima (in Radian). The average crystallite size obtained from the XRD analysis is reported in Table 2.

Theoretical X-ray density (d_x) for all the samples was calculated by the following equation;

$$d_x = \frac{2M}{Na^3} \text{ g/cm}^3 \quad (2)$$

where all the parameters have their usual meanings. The experimental bulk density (d_{exp}) for all the samples was calculated by Archimedes principle using Xylene as buoyant liquid. The porosity was also calculated using the equation;

$$\text{Porosity (\%)} = \left(1 - \frac{d_{exp}}{d_x}\right) \times 100 \quad (3)$$

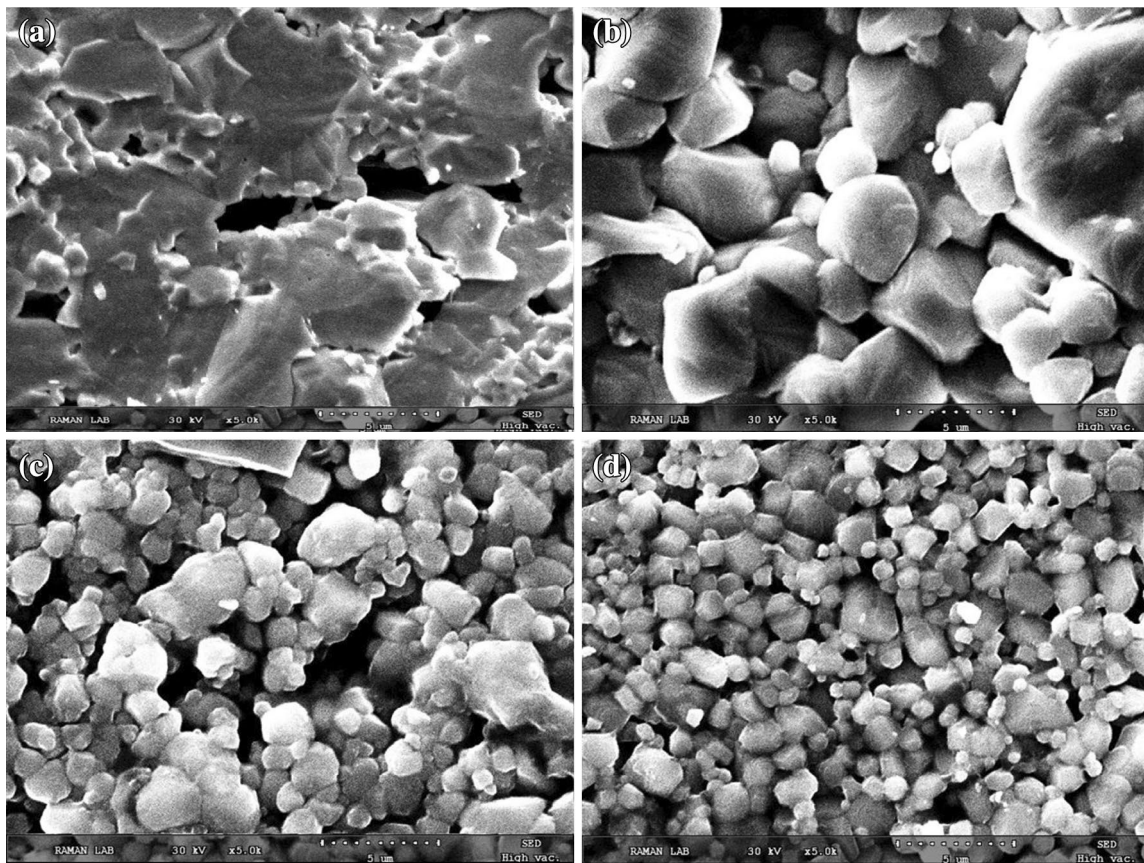


Fig. 3 SEM images of fractured surfaces of **a** CCTO, **b** CCTO1, **c** CCTO2 and **d** CCTO3, ceramics

The calculated values of all the parameters are summarized in Table 2.

Figure 3a–d shows the SEM micrographs of the fractured surface of all the CCTO compositions. Images clearly indicated that the presence of dopants strongly influenced the microstructure. The mean grain size of the doped CCTO was decreased with increase in subsequent concentrations of Zr^{4+} ions. For undoped CCTO, the abnormal grain formation was appeared which usually occurs due to presence of CuO/Cu_2O liquid phase formation at grain boundaries due to high temperature sintering process [35]. With subsequent doping of Nd and Zr in CCTO lattice, the grain growth is suppressed and normal grain matrix starts to appear. These observations indicate that the grain growth of the system was strongly controlled by of Zr^{4+} ions due to solute drag effect. As per solute theory substituted aliovalent ion with larger radii than host ion strongly segregate at grain boundaries and restricts the grain boundary movement. The similar microstructure observation was also reported earlier [36]. The average grain size for all the samples are listed in Table 2. The chemical composition and purity of product was confirmed through EDX technique. As illustrated in Fig. 4a–e, pure CCTO

ceramic composed of three different elements, Ca, Cu and Ti whereas, Nd and Zr co-doped CCTO ceramics have five different elements, Ca, Nd, Cu, Ti, and Zr. Furthermore, no impurity peaks were seen which indicate high purity of as-prepared CCTO ceramics.

3.2 Impedance spectroscopy

In the present section, we undertook the impedance analysis for the synthesized ceramics for revealing the effect of dopants on electrical properties and to recognize the various transport mechanisms existing within the material. Figure 5 shows the simulated complex impedance plane plots at 303 K for pure and doped CCTO compositions. The Nyquist plots elucidate that all samples exhibit single semicircular arc in the measured frequency range, which may be resultant of two or more relaxation process, respectively. Generally, high frequency semicircular arc identifies as bulk contribution, whereas the arc at intermediate frequencies ascribes as GBs response, while an electrode interface effect commonly appears at very low frequency domain. For all the synthesized ceramics, a single semicircular arc appears

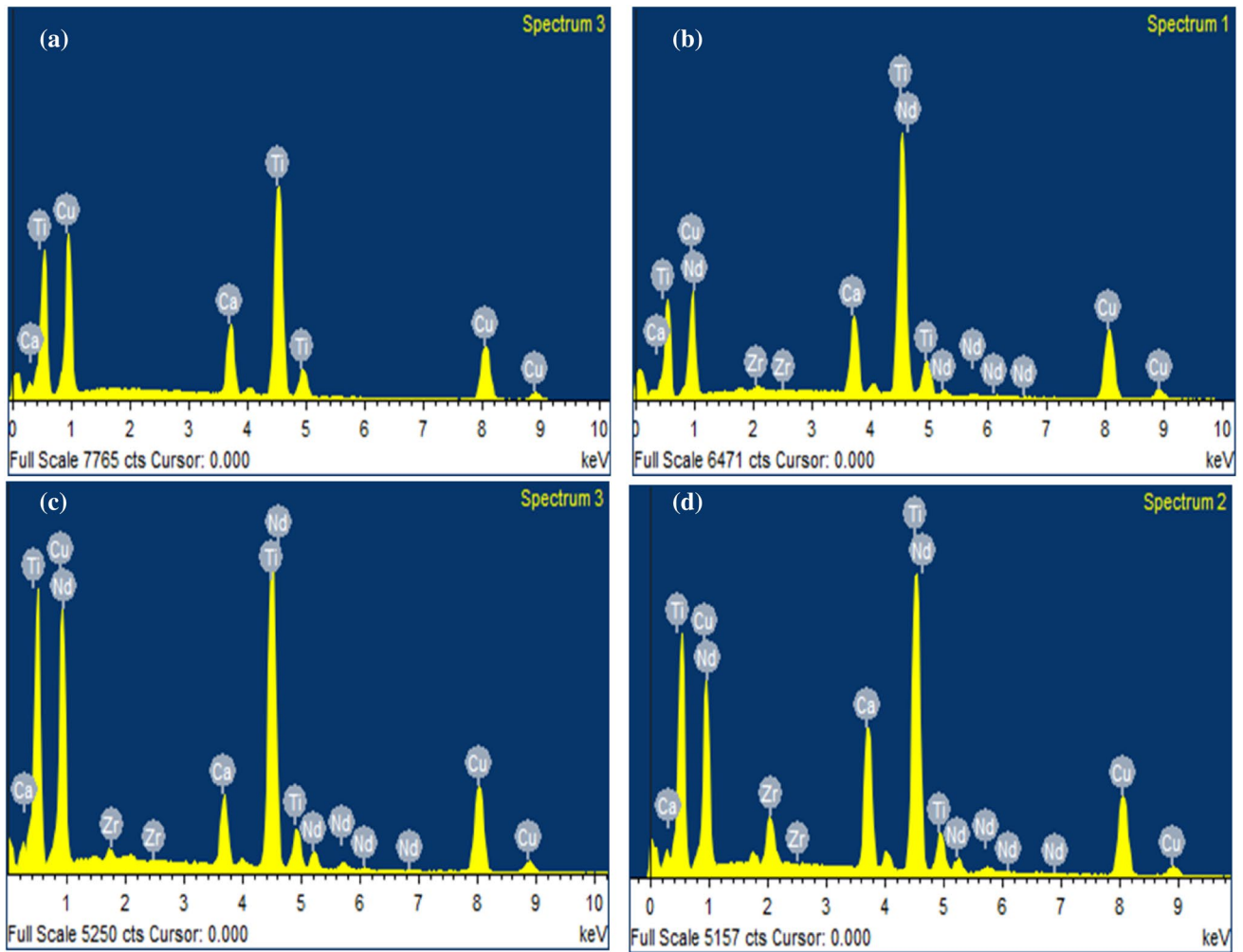


Fig. 4 EDX pattern of fractured surfaces of a CCTO, b CCTO1, c CCTO2 and d CCTO3, ceramics

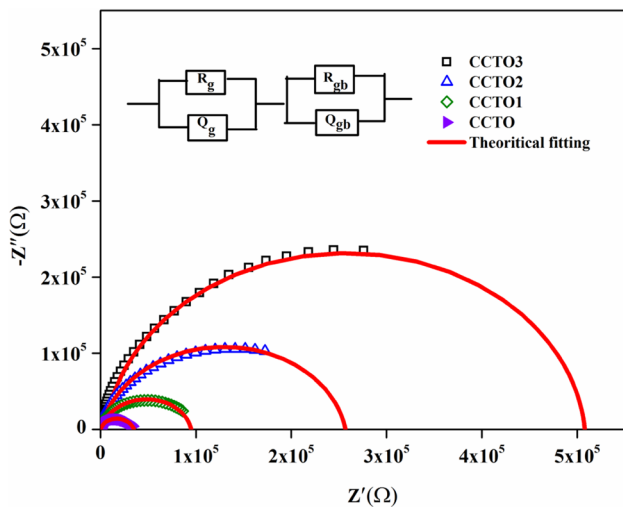


Fig. 5 Nyquist plots fitted to the 2R-CPE equivalent circuit model for pure CCTO and doped CCTO compositions at temperature 303 K

and the diameter of arc continuously increases with subsequent doping of Zr^{4+} ions in CCTO lattice. To facilitate the exact information about the contribution of grain and grain boundaries to the total dielectric response, impedance data were simulated using two R-CPE equivalent circuit model. CPE has been adopted instead of conventional capacitance (C) to accommodate the non-ideality of the system, which might be due to multiple relaxation time, non-uniform current distribution and surface roughness [37]. The frequency dependence of real and imaginary part of the impedance of the equivalent circuit can be expressed as [38].

$$Z' = \frac{R_g}{1 + (\omega R_g C_g)^2} + \frac{R_{gb}}{1 + (\omega R_{gb} C_{gb})^2}$$

$$Z'' = \frac{\omega R_g^2 C_g}{1 + (\omega R_g C_g)^2} + \frac{\omega R_{gb}^2 C_{gb}}{1 + (\omega R_{gb} C_{gb})^2}$$
(4)

where R_g and C_g are grain resistance and capacitance, respectively, and R_{gb} and C_{gb} are the corresponding quantities for grain boundary.

The capacitance of CPE can be calculated using the relationship;

$$C = Q^{1/n} R^{(1-n)/n} \quad (5)$$

where the value of n represents ideality (Debye or non-Debye behaviour) of the system. The calculated parameters [resistances (R_g , R_{gb}) and CPEs (Q_g , Q_{gb})] of fitted equivalent circuit are listed in Table 3. Further, looking at table results it is clear that grain resistance continuously decreases and GBs resistance increases with subsequent doping of Zr^{4+} ions. The GBs resistance value is approximately 10 times of magnitudes of grains resistance which signifies that the system are electrically heterogenous and approaches to IBLC structure. Therefore, impedance results suggest that the dielectric response of the investigated system may be accredited to IBLC effect.

3.3 Dielectric properties

Figure 6a, b represents the frequency dependent behaviour of ϵ' and $\tan \delta$ at room temperature for all the compositions. It is clear that all the sample exhibits low frequency dielectric dispersion with high value of ϵ' is attributed due to Maxwell–Wanger effect or can be understood with Koop's theory [39, 40]. The impedance spectroscopy also identifies the co-existence of insulating regions (GBs) with less resistive regions (grains) results to the dielectric heterogeneity. In the low frequency domain, the charge carriers cannot migrate easily through highly resistive grain boundaries and piles up in interfacial layers gives rise to strong polarization and result in enhanced values of ϵ' . At high frequencies the decrease in ϵ' is observed due to lack of ability of electric dipoles to switch with the applied electric field leading to a lower dipolar response. According to Koop's model, at lower frequencies high energy is required by the charge carriers to move across the resistive GBs and leads to high $\tan \delta$ values. Pure CCTO exhibits frequency independent plateau

Table 3 The values of parameters Q_g , Q_{gb} , R_g , R_{gb} , n_g and n_{gb} associated with grains, grain boundaries calculated by simulating Nyquist plots using 2R-CPE equivalent circuit model at room temperature

| Sample | R_g (Ω) | Q_g | n_g | R_{gb} (Ω) | Q_{gb} | n_{gb} |
|--------|--------------------|-----------------------|-------|-----------------------|-----------------------|----------|
| CCTO | 8000 | 8.0×10^{-8} | 0.80 | 3.2×10^4 | 6.28×10^{-7} | 0.89 |
| CCTO1 | 5200 | 7.0×10^{-8} | 0.85 | 9.0×10^4 | 8.70×10^{-7} | 0.90 |
| CCTO2 | 3740 | 1.49×10^{-7} | 0.77 | 2.5×10^5 | 9.21×10^{-7} | 0.97 |
| CCTO3 | 1290 | 4.60×10^{-8} | 0.79 | 5.0×10^5 | 1.81×10^{-6} | 0.95 |

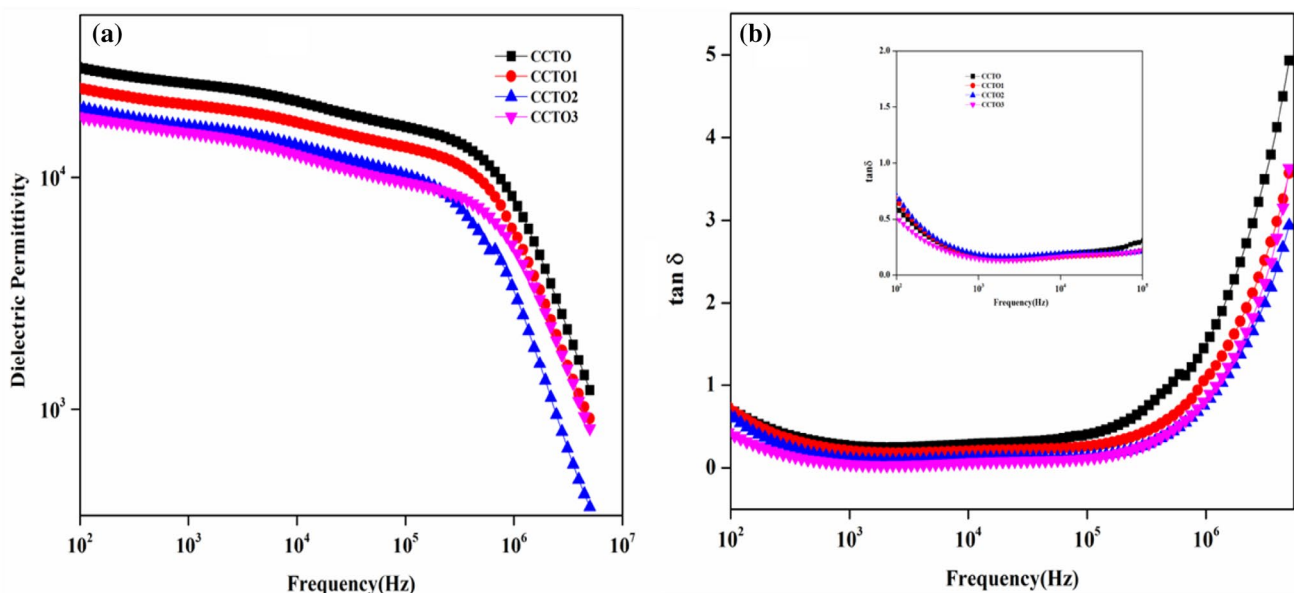


Fig. 6 Frequency dependence of **a** ϵ' and **b** $\tan \delta$ for all the compositions at room temperature. Inset of **b** represents the zoom view of $\tan \delta$ (for all the ceramics in the frequency range of 10^2 – 10^5 Hz)

with giant ϵ' value and a sudden drop in ϵ' over 400 kHz might be due to the conductive nature of grains [41]. The giant value of $\epsilon' \sim 25,345$ at 1 kHz for undoped CCTO drops to $\epsilon' \sim 16,902$ for CCTO3 by addition of Nd^{3+} and Zr^{4+} ions in lattice, but the high frequency relaxation shifted toward higher frequencies which is a desirable feature for device applications. The decrease in dielectric permittivity may attributed to decrease in grain size which can be explained by IBLC model introduced by Adams et al. [42]. As per this model, the dielectric permittivity can be correlated to the average grain size and thickness of grain boundary is given by the relationship as follow;

$$\epsilon_{\text{eff}} = \frac{t_g}{t_{\text{gb}}} \epsilon_r \quad (6)$$

where t_g represents the mean grain size and t_{gb} corresponds to the grain boundary thickness. Equation (1) suggests that the effective dielectric permittivity is directly related to grain size and inversely related to grain boundary thickness. Due to the large number of grain boundaries embedded in the pool of the grains in polycrystalline materials, it is very difficult to analyse the impact of grain boundary thickness of ϵ' and hence the grain size effect dominates to determine the effective dielectric permittivity. Therefore, the observed dielectric behaviour of the present system can be explained by the grain size effect. Further, the charge compensation is required for lattice neutralization due to replacement of Ca^{2+} by Nd^{3+} ions in CCTO matrix. This charge compensation may preserve the large value of ϵ' and prevents the proportionate drop in dielectric constant values with a decrease in grain size. The investigated system was valuable only their dielectric losses were also controlled. As shown in Fig. 5b, the $\tan\delta$ spectra are similar for all the compositions, but values of $\tan\delta$ are different significantly. Especially, for the CCTO3 composition, the value of $\tan\delta$ is less than 0.10 in wide frequency range 1–200 kHz with the minimal value of 0.031 at 2.1 kHz at room temperature which is 85% lower than that of undoped CCTO. Zr^{4+} has larger ionic radii than Ti^{4+} , the significant size mismatch between these cations cause a strong driving force that segrate Zr^{4+} ions at grain boundaries which enhances the GBs resistance. This was primarily due to enhanced GB density occurring from reduction in the mean grain size by the solute drag effect. The trend of R_{gb} is well supported with observed $\tan\delta$ spectra and enhanced R_{gb} values are responsible for low loss over a broad range of frequencies (inset Fig. 5b). The low value of $\tan\delta$ with high ϵ' value in wide frequency region is greatly desired for energy storage technologies. Therefore, the studied system can be very useful for practical applications.

4 Conclusion

Nd and Zr modified CCTO ceramics were successfully synthesized by conventional solid state route. The XRD analysis confirmed that all the modified CCTO ceramics remained cubic in structure. The variation in lattice parameters and unit cell volume analyzed by Rietveld refinement of XRD data surely indentified that the substituted dopants successfully incorporated in CCTO lattice. Analysis of SEM images revealed that microstructure was strongly affected by Nd and Zr co-substitution and its direct impact reflected on dielectric properties. A huge value of dielectric permittivity ($\epsilon_r \sim 16,902$) with nominal dielectric losses ($\tan\delta \sim 0.067$ at 1 kHz) was observed in a broad frequency range from 10^3 to 10^5 Hz for CCTO3 ceramic. Thus, it is concluded that the both dopant ions have played an independent role to improve the dielectric performance of CCTO system. A' site Ca substitution by Nd may be attributed to enhancement in dielectric permittivity, and Zr ions suppressed the grain growth and yielded a high resistive GBs network that strongly favours the improved the dielectric performance of CCTO system.

Acknowledgements Authors are thankful to Department of Science and Technology, New Delhi for providing XRD facilities (FIST scheme). One of the author is thankful to the University Grants Commission, New Delhi for providing financial assistance through major research project (F. No. 41-853/2012 (SR)).

References

1. M.A. Subramanian, D. Li, N. Duan, B.A. Reisner, A.W. Sleight, High dielectric constant in $\text{ACu}_3\text{Ti}_4\text{O}_{12}$ and $\text{ACu}_3\text{Ti}_3\text{FeO}_{12}$ phases. *J. Solid State Chem.* **151**, 323–325 (2000)
2. M.M. Ahmad, E. Al-Libidi, A. Al-Jaafari, S. Ghazanfar, K. Yamada, Mechanochemical synthesis and giant dielectric properties of $\text{CaCu}_3\text{Ti}_4\text{O}_{12}$. *Appl. Phys. A* **116**, 1299–1306 (2014)
3. V.P.B. Marques, A. Ries, A.Z. Simoes, M.A. Ramirez, J.A. Varela, E. Longo, Evolution of $\text{CaCu}_3\text{Ti}_4\text{O}_{12}$ varistor properties during heat treatment in vacuum. *Ceram. Int.* **33**, 1187–1190 (2007)
4. S. G-Fritsch, T. Lebey, M. Boulous, B. Durand, Dielectric properties of $\text{CaCu}_3\text{Ti}_4\text{O}_{12}$ based multiphased ceramics. *J. Eur. Ceram. Soc.* **26**, 1245–1257 (2006)
5. M.A. de la Rubia, P. Leret, A. Del Campo, R.E. Alonso, A.R. Lopez-Garcia, J.F. Fernandez, J. De Frutos, Dielectric behaviour of Hf-doped $\text{CaCu}_3\text{Ti}_4\text{O}_{12}$ ceramics obtained by conventional synthesis and reactive sintering. *J. Eur. Ceram. Soc.* **32**, 169–1699 (2012)
6. W.M. Hua, Z. Fu, W.Q. Li, Y. Chao, Synthesis of $\text{CaCu}_3\text{Ti}_4\text{O}_{12}$ powders and ceramics by sol-gel method using decanedioic acid and its dielectric properties. *J. Cent. South Univ.* **19**, 3385–3389 (2012)
7. N. Banerjee, S.B. Krupanidhi, Low temperature synthesis of nanocrystalline $\text{CaCu}_3\text{Ti}_4\text{O}_{12}$ through a fuel mediated autocombustion pathway. *Curr. Nanosci.* **6**, 432–438 (2010)
8. M. Eghbali-Arani, A. Sobhani-Nasab, M. Rahimi-Nasrabadi, F. Ahmadi, S. Pourmasoud, Ultrasound-assisted synthesis of YbVO_4

- nanostructure and $\text{YbVO}_4/\text{CuWO}_4$ nanocomposites for enhanced photocatalytic degradation of organic dyes under visible light. *Ultrason. Sonochem.* **43**, 120–135 (2018)
9. S. Pourmasoud, A. Sobhani-Nasab, M. Behpour, M. Rahimi-Nasrabadi, F. Ahmadi, Investigation of optical properties and the photocatalytic activity of synthesized YbVO_4 nanoparticles and $\text{YbVO}_4/\text{NiWO}_4$ nanocomposites by polymeric capping agents. *J. Mol. Struct.* **1157**, 607–615 (2018)
 10. M. Salavati-Niasari, F. Soofivand, A. Sobhani-Nasab, M. Shakkouri-Arani, M. Hamadani, S. Bagheri, Facile synthesis and characterization of CdTiO_3 nanoparticles by Pechini sol-gel method. *J. Mater. Sci.: Mater. Electron.* **28**, 14965–14973 (2017)
 11. A. Sobhani-Nasab, A. Ziarati, M. Rahimi-Nasrabadi, M.R. Ganjali, A. Badiei, Five-component domino synthesis of tetrahydropyridines using hexagonal $\text{PbCr}_x\text{Fe}_{12-x}\text{O}_{19}$ as efficient magnetic nanocatalyst. *Res. Chem. Intermed.* **43**, 6155–6165 (2017)
 12. S.S. Hosseinpour-Mashkani, A. Sobhani-Nasab, Investigation the effect of temperature and polymeric capping agents on the size and photocatalytic properties of NdVO_4 nanoparticles. *J. Mater. Sci.: Mater. Electron.* **28**, 16459–16466 (2017)
 13. S. Vangchangya, E. Swatsitang, P. Thongbai, S. Pinitsoontorn, T. Yamwong, S. Maensiri, V. Amornkitbamrung, P. Chindaprasirt, Very low loss tangent and high dielectric permittivity in pure- $\text{CaCu}_3\text{Ti}_4\text{O}_{12}$ ceramics prepared by a modified sol-gel process. *J. Am. Ceram. Soc.* **95**, 1497–1500 (2012)
 14. R. Kashyap, O.P. Thakur, R.P. Tandon, Study of structural, dielectric and electrical conduction behaviour of Gd substituted $\text{CaCu}_3\text{Ti}_4\text{O}_{12}$ ceramics. *Ceram. Int.* **38**, 3029–3037 (2012)
 15. L. Feng, X. Tang, Y. Yan, X. Chen, Z. Jiao, G. Cao, Decrease of dielectric loss in $\text{CaCu}_3\text{Ti}_4\text{O}_{12}$ ceramics by La doping. *Phys. Status Solidi A* **203**, R22–R24 (2006)
 16. C.H. Mu, P. Liu, Y. He, J.P. Zhou, H.W. Zhang, An effective method to decrease dielectric loss of $\text{CaCu}_3\text{Ti}_4\text{O}_{12}$ ceramics. *J. Alloys Compd.* **471**, 137–141 (2009)
 17. R. Kumari, N. Ahlawat, A. Agarwal, S. Sanghi, M. Sindhu, S. Rani, Effect of doping of alkaline metal ions on structural and electrical properties of $\text{Bi}_{0.8}\text{M}_{0.2}\text{FeO}_3$ -modified $\text{Na}_{0.5}\text{Bi}_{0.5}\text{TiO}_3$ ceramics ($M = \text{Ca}, \text{Sr}$, and Ba). *J. Alloys Compd.* **747**, 712–720 (2018)
 18. B. Castor, B. James Hedrick, in *Industrial Minerals and Rocks*, ed. by J. E. Kogel, N. C. Trivedi, J. M. Barker (Society for mining, Metallurgy, and Exploration, United State, 2006), pp. 769–792
 19. L. Liu, L. Fang, Y. Huang, Y. Li, D. Shi, S. Zheng, S. Wu, C. Hu, Dielectric and nonlinear current–voltage characteristics of rare-earth doped $\text{CaCu}_3\text{Ti}_4\text{O}_{12}$ ceramics. *J. Appl. Phys.* **110**, 094101 (2011)
 20. L. Feng, X. Tang, Y. Yan, X. Chen, Z. Jiao, G. Cao, Decrease of dielectric loss in $\text{CaCu}_3\text{Ti}_4\text{O}_{12}$ ceramics by La doping. *Phys. Status Solidi (a)* **203**, R22 (2006)
 21. B.S. Prakash, K.B.R. Varma, Microstructural and dielectric properties of donor doped (La^{3+}) $\text{CaCu}_3\text{Ti}_4\text{O}_{12}$ ceramics. *J. Mater. Sci. Mater. Electron.* **17**, 899–907 (2006)
 22. T. Li, Y. Xue, Z. Chen, F. Chang, Dielectric characteristics and positron annihilation study of Eu_2O_3 -doped $\text{CaCu}_3\text{Ti}_4\text{O}_{12}$ ceramics. *Mater. Sci. Eng. B* **158**, 58–62 (2009)
 23. C. Mu, H. Zhang, Y. Liu, Y. Song, P. Liu, Rare earth doped $\text{CaCu}_3\text{Ti}_4\text{O}_{12}$ electronic ceramics for high frequency applications. *J. Rare Earths* **28**, 43–47 (2010)
 24. J. Boonlakhorn, P. Thongbai, B. Putasaeng, T. Yamwong, S. Maensiri, Very high-performance dielectric properties of $\text{Ca}_{1-3x/2}\text{Yb}_x\text{Cu}_3\text{Ti}_4\text{O}_{12}$ ceramics. *J. Alloys Compd.* **612**, 103–109 (2014)
 25. J. Li, B. Fu, H. Lu, C. Huang, J.W. Sheng, Dielectric properties of Sm-doped $\text{CaCu}_3\text{Ti}_4\text{O}_{12}$ ceramics. *Ceram. Int.* **39**, S149–S152 (2013)
 26. Z. Xu, H. Qiang, Y. Chen, Z. Chen, Microstructure and enhanced dielectric properties of yttrium and zirconium co-doped $\text{CaCu}_3\text{Ti}_4\text{O}_{12}$ ceramics. *Mater. Chem. Phys.* **191**, 1–5 (2017)
 27. Y. Wang, L. Ni, X.M. Chen, Effects of Nd-substitution on microstructures and dielectric characteristics of $\text{CaCu}_3\text{Ti}_4\text{O}_{12}$ ceramics. *J. Mater. Sci.: Mater. Electron.* **22**, 345–350 (2012)
 28. M.H. Wang, B. Zhang, F. Zhou, C. Yao, Microstructure and dielectric properties of Nd doped $\text{CaCu}_3\text{Ti}_4\text{O}_{12}$ synthesized by sol-gel method. *J. Sol-Gel. Sci. Technol.* **69**, 281–287 (2014)
 29. S. Mahajan, O.P. Thakur, C. Prakash, K. Sreenivas, Effect of Zr on dielectric, ferroelectric and impedance properties of BaTiO_3 ceramic. *Bull. Mater. Sci.* **34**, 1483–1489 (2011)
 30. K.M. Sangwan, N. Ahlawat, R.S. Kundu, S. Rani, S. Rani, N. Ahlawat, Improved dielectric and ferroelectric properties of Mn doped Barium zirconium titanate (BZT) ceramics for energy storage applications. *J. Phys. Chem. Solids* **117**, 158–166 (2018)
 31. Q.G. Chi, L. Gao, X. Wang, J.Q. Lin, J. Sun, Q. Lei, Effects of Zr doping on the microstructures and dielectric properties of $\text{CaCu}_3\text{Ti}_4\text{O}_{12}$ ceramics. *J. Alloys Compd.* **559**, 45–48 (2013)
 32. K.M. Sangwan, N. Ahlawat, R.S. Kundu, S. Rani, S. Rani, N. Ahlawat, Influence of Mn doping on electrical conductivity of lead free BaZrTiO_3 perovskite ceramic. *Cer. Int.* <https://doi.org/10.1016/j.ceramint.2018.03.039>
 33. S. Rani, N. Ahlawat, R.S. Kundu, R. Punia, S. Kumar, K.M. Sangwan, N. Ahlawat, Structural and dielectric properties of $\text{Ca}_{0.95}\text{Nd}_{0.05}\text{Cu}_3\text{Ti}_{3.95}\text{Zr}_{0.05}\text{O}_{12}$ ceramic. *Ferroelectrics* **516**, 156–166 (2017)
 34. J.R. Carvajal, Recent advances in magnetic structure determination by neutron powder diffraction. *Phys. B* **192**, 55–69 (1993)
 35. D.W. Kim, T.G. Kim, F.S. Hong, Low firing of CuO-doped anatase. *Mater. Res. Bull.* **34**, 771–781 (1999)
 36. L.J. Liu, Y.M. Huang, Y.H. Li, D.P. Shi, S.Y. Zheng, S.S. Wu, L. Fang, C.Z. Hu, Dielectric and non-Ohmic properties of $\text{CaCu}_3\text{Ti}_4\text{O}_{12}$ ceramics modified with NiO , SnO_2 , SiO_2 , and Al_2O_3 additives. *J. Mater. Sci.* **47**, 2294–2299 (2012)
 37. S. Rani, N. Ahlawat, R. Punia, K.M. Sangwan, S. Rani, Dielectric relaxation and conduction mechanism of complex perovskite $\text{Ca}_{0.90}\text{Sr}_{0.10}\text{Cu}_3\text{Ti}_{3.95}\text{Zn}_{0.05}\text{O}_{12}$ ceramic. *Ceram. Int.* **44**, 5996–6001 (2018)
 38. J. Liu, C. Duan, W.N. Mei, R.W. Smith, J.R. Hardy, Dielectric properties and Maxwell–Wagner relaxation compounds $\text{ACaCu}_3\text{Ti}_4\text{O}_{12}$ ($A = \text{Ca}, \text{Bi}_{2/3}, \text{Y}_{2/3}, \text{La}_{2/3}$). *J. Appl. Phys.* **98**, 093703 (2005)
 39. J.C. Maxwell, *Electricity and Magnetism*, 1st edn. (Oxford University Press, Oxford, 1929)
 40. C.G. Koons, On the dispersion of resistivity and dielectric constant of some semiconductors at audiofrequencies. *Phys. Rev.* **83**, 121–124 (1951)
 41. T.B. Adams, D.C. Sinclair, A.R. West, Giant barrier layer capacitance effects in $\text{CaCu}_3\text{Ti}_4\text{O}_{12}$ ceramics. *Adv. Mater.* **14**, 1321 (2002)
 42. T.B. Adams, D.C. Sinclair, A.R. West, Characterization of grain boundary impedances in fine-and coarse-grained $\text{CaCu}_3\text{Ti}_4\text{O}_{12}$ ceramics. *Phys. Rev. B* **73**, 94124–94126 (2009)